Deuteron-induced reactions on Ni isotopes up to 60 MeV

M. Avrigeanu,[1,*] E. Šimečková,[2,†] U. Fischer,[3] J. Mrázek,[2] J. Novak,[2] M. Štefánik,[2] C. Costache,[1] and V. Avrigeanu[1]

[1]*Horia Hulubei National Institute for Physics and Nuclear Engineering, P.O. Box MG-6, R-077125 Bucharest-Magurele, Romania*

[2]*Nuclear Physics Institute CAS, CZ-25068 Řež, Czech Republic*

[3]*Euratom/FZK Fusion Association, Karlsruhe Institute of Technology (KIT), Hermann-von-Helmholtz-Platz, 1, D-76344 Eggenstein-Leopoldshafen, Germany*

(Received 11 June 2016; published 12 July 2016)

Background: The high complexity of the deuteron-nucleus interaction from the deuteron weak binding energy of 2.224 MeV is also related to a variety of reactions induced by the deuteron-breakup (BU) nucleons. Thus, specific noncompound processes as BU and direct reactions (DR) make the deuteron-induced reactions so different from reactions with other incident particles. The scarce consideration of only pre-equilibrium emission (PE) and compound-nucleus (CN) mechanisms led to significant discrepancies with experimental results so that recommended reaction cross sections of high-priority elements as, e.g., Ni have mainly been obtained by fit of the data.

Purpose: The unitary and consistent BU and DR account in deuteron-induced reactions on natural nickel may take advantage of an extended database for this element, including new accurate measurements of particular reaction cross sections.

Method: The activation cross sections of ^{64,61,60}Cu, ^{65,57}Ni, and ^{55,56,57,58,58m,60}Co nuclei for deuterons incident on natural Ni at energies up to 20 MeV, were measured by the stacked-foil technique and high-resolution gamma spectrometry using U-120M cyclotron of CANAM, NPI CAS. Then, within an extended analysis of deuteron interactions with Ni isotopes up to 60 MeV, all processes from elastic scattering until the evaporation from fully equilibrated compound system have been taken into account while an increased attention is paid especially to the BU and DR mechanisms.

Results: The deuteron activation cross-section analysis, completed by consideration of the PE and CN contributions corrected for decrease of the total-reaction cross section from the leakage of the initial deuteron flux towards BU and DR processes, is proved satisfactory for the first time to all available data.

Conclusions: The overall agreement of the measured data and model calculations validates the description of nuclear mechanisms taken into account for deuteron-induced reactions on Ni, particularly the BU and DR that should be considered explicitly.

DOI: 10.1103/PhysRevC.94.014606

I. INTRODUCTION

The extended database for deuteron-induced reactions on natural nickel at low energies offered a good opportunity to continue the series of recent analyses [1–5] looking for the consistent inclusion of the deuteron breakup (BU) contribution within activation cross-section calculations. While the description of deuteron-nucleus interaction represents an important test for the reaction mechanism models, because of the weak deuteron binding energy of 2.224 MeV and the variety of reactions initiated by the BU nucleons, the eventual key role of BU and direct processes for deuterons on Ni may fill in the recent similar discussion including the Fe and Cu stable isotopes [6,7].

On the other hand, the above-mentioned significant database exists because nickel is an important structural, alloying, and surface coating material used in nuclear technology while isotopes of Ni are also used for the production of diagnostic and therapeutic radioisotopes. However, there are yet contradicting experimental data for several reactions whereas the related model calculations were recently proved to need improvements to enhance the quantitative prediction of data [8,9]. It is why the presently recommended cross sections of deuteron-induced reactions on natural nickel have mainly been obtained by fit of the measured data [8–10]. Therefore, complementary cross-section measurements as well as further model calculations are necessary to meet the demands of several ongoing strategic research programs at international large-scale facilities [11–13] and databases [14].

Consequently, the present work aims both to strengthen the database of deuteron-induced reactions on natural nickel, up to 20 MeV, and a deeper understanding of deuteron breakup and very poorly taken into account (d,p) and (d,n) stripping as well as the (d,t) and (d,α) pick-up direct reactions (DRs), all together and consistently with the well-established statistical emission. The experimental setup and the measured data are described in Sec. II. Next, a consistent energy-dependent optical potential for deuteron on Ni isotopes is first discussed in Sec. III A. Deuteron breakup effects on the corresponding activation cross sections of Ni isotopes are the subject of Sec. III B, while the DR analysis using the computer code FRESCO [15] is described in Sec. III C as well as the pre-equilibrium (PE) and emission from fully equilibrated compound nucleus (CN) contributions, using the

*marilena.avrigeanu@nipne.ro

†simecek@ujf.cas.cz

code TALYS-1.8 [16], in Sec. III D. The measured and calculated deuteron activation cross sections of Ni stable isotopes and natural Ni are compared in Sec. IV, including the evaluated data from the TENDL-2015 library [17], and conclusions of this work are given in Sec. V.

II. MEASUREMENTS

The irradiation was carried out on CANAM infrastructure of NPI CAS using an external deuteron beam of the variable-energy cyclotron U–120M operating in the negative-ion mode. The beam was extracted using a stripping-foil extractor and was delivered to the reaction chamber through a beam line consisting of one dipole and two quadrupole magnets. The mean beam energy was determined with an accuracy of 1%, with full width at half maximum (FWHM) of 1.8%.

The activation cross sections were measured by the stacked-foil technique. The collimated deuteron beam impinged the stack of foils placed in a cooled reaction chamber, that served also as a Faraday cup. Accuracy of the current and charge measurement was 5%.

The high-purity Ni foils (Goodfellow product—99.9% purity, 25 μm declared thickness) and Al (50 μm declared thickness) were weighed (within 2% of accuracy) to avoid relatively large uncertainties in the foil thickness declared by the producer. The mean energy, energy thickness, and energy spread in each foil were simulated by the SRIM 2008 package [18]. The Ni foils were interleaved with Al foils that were used for additional monitoring of the beam current and deuteron energy loss as well.

Natural nickel consists of five stable isotopes: ^{58}Ni (68.08%), ^{60}Ni (26.22%), ^{61}Ni(1.14%), ^{62}Ni (3.64%), and ^{64}Ni (0.93%) which leads to many open reaction channels. The irradiation was carried up in three runs to check an internal consistency of the measurement. The characteristics of the single runs are given in Table I.

The gamma rays from the irradiated foils were measured repeatedly by two calibrated high-purity germanium (HPGe) detectors of 50% efficiency and FWHM of 1.8 keV at 1.3 MeV; one of them (with Be window) was calibrated to low energy by gamma rays (53.161 keV) and x rays (30.973 keV, 30.625 keV, and 34.987 keV) from the ^{133}Ba standard. Experimental reaction rates were calculated from the specific activities at the end of the irradiation and corrected to the decay during irradiation using the charge measurement and foil characteristics as well. The measurement with different cooling times lasted up to 100 days after irradiation. The decay data of the isotopes observed from irradiated Ni foils [19] are given in Table II. A background contribution was extracted from the lines 1115.55 keV, 1377.63 keV, 1332.5 keV, and 1273.24 keV.

TABLE I. Characteristics of single runs.

Run no.	Initial energy (MeV)	Total charge (μC)	Irradiation time (s)	Mean current (μA)
1	19.93	65.65	432	0.152
2	19.93	69.72	433	0.161
3	19.48	154.55	482	0.321

TABLE II. Half-lives, main gamma lines, and their intensities [19] of the isotopes observed from irradiated Ni foils.

Isotope	$T_{1/2}$	E_γ(keV)	I_γ(%)
^{64}Cu	12.7 h	1345.84	0.473
^{61}Cu	3.333 h	282.96	12.2
		656.01	10.77
		1185.23	3.75
^{60}Cu	23.7 min	1791.6	45.4
		826.06	21.7
^{65}Ni	2.5172 h	1481.84	24
		1115.55	15.43
^{57}Ni	35.6 h	1377.63	81.7
		127.16	16.7
^{60}Co	5.2714 year	1332.5	99.99
		1173.24	99.97
^{58}Co	70.86 day	810.78	99
^{58}Co^m	9.04 h	24.89	0.0389
^{57}Co	271.79 day	122.06	85.6
		136.47	10.68
^{56}Co	77.27 day	846.77	100
		1771.35	15.69
^{55}Co	17.53 h	931.3	75
		477.2	20.2

The experimental cross sections of the Ni$(d,x)^{64}$Cu, Ni$(d,x)^{61}$Cu, Ni$(d,x)^{60}$Cu, Ni$(d,x)^{65}$Ni, Ni$(d,x)^{57}$Ni, Ni$(d,x)^{60}$Co, Ni$(d,x)^{58}$Co, Ni$(d,x)^{58}$Co^m, Ni$(d,x)^{57}$Co, Ni$(d,x)^{56}$Co, and Ni$(d,x)^{55}$Co reactions are shown in Table III. However, the isotope ^{65}Ni is populated only via ^{64}Ni(d,p) reaction, so the corresponding cross section is directly related to the natural Ni by an abundance factor. Similar situation is for the ^{58}Ni$(d,x)^{57}$Ni, ^{58}Ni$(d,x)^{56}$Co, and ^{58}Ni$(d,x)^{55}$Co reactions at energies below 20 MeV. The same residual nuclei are also populated through reactions on ^{60}Ni above the incident energy of 20 MeV. The measured cross sections are in good agreement with recent data [8–10,20–26] and will be discussed in Sec. IV.

The cross section for production of ^{61}Co up to 20 MeV was not determined in present work. The reason is that all three gamma lines in ^{61}Co decay ($T_{1/2} = 1.650$ h), i.e., 67.412 keV (85%), 908.631 keV (3.6%), and 841.21 keV (0.79%), are also present in ^{61}Cu decay ($T_{1/2} = 3.333$ h) to the same daughter nucleus ^{61}Ni. The time dependence of activity and the relative intensities of these lines are consistent with ^{61}Cu decay. The upper limit for the Ni$(d,x)^{61}$Co reaction is in the order of present experimental errors and thus the contribution of ^{61}Co decay to the observed activity is not significant below 20 MeV (see Fig. 13).

The ^{58}Co nucleus ($T^g_{1/2} = 70.86$ d) has a long-living metastable isomer ^{58}Co^m ($T^m_{1/2} = 9.04$ h) decaying through the 24.9 keV ($I = 0.0389\%$) gamma ray to the ground state. This isomer feeds the ^{58}Co^g ground state by 100% of intensity. Thus the cumulative cross section (isomeric and ground state) was measured after a period of time of $\sim$10 $T^m_{1/2}$.

TABLE III. Measured reaction cross sections (mb) for deuterons incident on natural nickel. The energy errors take into account the energy thickness of each foil and the initial-energy spread error. Cross-section errors are composed of statistical errors in activity determination and systematical errors of charge measurement uncertainty (∼5%), foil thickness uncertainty (2%), and uncertainty of HPGe detector efficiency determination (2%). The uncertainties are given in parentheses, in units of the last digit.

Energy	Reaction										
(MeV)	Ni(d,x)^{64}Cu	Ni(d,x)^{61}Cu	Ni(d,x)^{60}Cu	Ni(d,x)^{65}Ni	Ni(d,x)^{57}Ni	Ni(d,x)^{60}Co	Ni(d,x)^{58}Co	Ni(d,x)^{58}Co^{m}	Ni(d,x)^{57}Co	Ni(d,x)^{56}Co	Ni(d,x)^{55}Co
19.59 (34)	6.47 (94)	16.67 (100)	45.60 (263)	0.789 (56)	6.57 (46)	10.25 (100)	265.3 (153)	193.1 (291)	101.8 (60)	9.56 (55)	19.37 (112)
19.25 (34)	6.35 (63)	17.86 (106)	53.62 (618)	0.907 (57)	5.71 (36)	9.58 (69)	276.0 (162)	183.2 (234)	87.12 (547)	10.42 (60)	19.35 (117)
18.39 (37)	7.74 (90)	16.20 (129)	48.48 (286)	0.888 (60)	4.75 (31)	8.60 (54)	264.1 (152)	214.7 (243)	65.87 (384)	10.90 (63)	16.74 (99)
18.24 (33)	8.09 (71)	18.91 (111)	54.89 (633)	0.975 (61)	4.44 (28)	9.09 (58)	272.0 (163)	186.2 (223)	62.46 (365)	11.45 (66)	16.59 (98)
17.14 (35)	8.64 (83)	19.61 (115)	42.50 (246)	1.03 (7)	3.70 (23)	6.38 (69)	261.5 (151)	212.7 (356)	42.33 (250)	13.74 (85)	13.92 (81)
15.85 (39)	9.86 (70)	23.24 (141)	38.61 (233)	1.28 (9)	2.95 (18)	5.00 (47)	246.8 (143)	207.4 (235)	32.80 (191)	16.15 (93)	11.13 (64)
15.83 (36)	9.27 (75)	22.85 (135)	49.36 (351)	1.18 (8)	2.87 (18)	4.96 (37)	255.8 (151)	197.0 (231)	32.74 (191)	16.51 (96)	11.09 (65)
14.67 (39)	10.14 (76)	25.76 (152)	40.35 (256)	1.37 (8)	2.34 (15)	3.06 (91)	246.7 (146)	188.0 (215)	26.59 (155)	20.9 (12)	8.69 (52)
14.51 (36)	9.59 (95)	25.33 (153)	27.65 (179)	1.33 (8)	2.35 (14)	3.45 (74)	237.9 (137)	188.1 (378)	23.72 (165)	21.6 (13)	8.12 (47)
13.11 (45)	9.42 (78)	29.90 (176)	17.35 (102)	1.53 (9)	1.51 (10)	0.62 (33)	205.1 (118)	149.9 (210)	15.92 (94)	27.6 (16)	4.27 (25)
11.90 (49)	8.64 (67)	32.77 (197)	7.34 (47)	1.66 (10)	0.699 (45)		169.1 (979)	133.6 (156)	8.73 (51)	32.3 (19)	1.53 (9)
11.73 (47)	9.28 (73)	36.70 (215)	11.50 (76)	1.78 (11)	0.796 (51)		181.4 (106)	144.0 (173)	9.16 (55)	34.6 (20)	1.56 (9)
11.52 (49)	7.58 (71)	36.25 (217)	6.31 (50)	1.81 (11)	0.658 (39)		164.6 (95)	148.6 (280)	6.77 (41)	36.2 (21)	0.953 (56)
10.27 (48)	8.08 (59)	44.91 (263)	1.78 (16)	2.11 (12)	0.249 (16)		127.3 (75)	102.1 (130)	3.01 (21)	38.6 (22)	0.211 (13)
10.15 (51)	7.66 (76)	43.84 (296)	0.90 (6)	2.00 (14)	0.214 (15)		112.4 (65)	89.4 (138)	2.51 (18)	38.4 (22)	0.155 (10)
9.81 (51)	6.90 (80)	48.10 (289)	0.34 (2)	2.07 (13)	0.120 (8)		94.2 (54)	79.0 (160)	1.43 (13)	37.3 (22)	0.056 (5)
7.84 (63)	3.98 (47)	57.58 (367)	0.09 (1)	2.47 (15)			30.0 (17)	16.1 (47)	0.24 (4)	28.4 (16)	0.008 (1)
5.35 (83)		46.26 (279)		2.02 (12)			6.14 (36)	2.25 (32)		10.24 (59)	
1.5 (15)		0.89 (5)		0.057 (4)			1.33 (9)			0.12 (1)	

The cross section of Ni(d,x)^{58}Co^{m} reaction was determined by the analysis of the dependence of 819.8 keV gamma-line activity on the measurement time. The specific activities A_m^0 (metastable) and A_g^0 (ground state) at the end of irradiation were determined using the MINUIT code [34] for minimization of the Bateman equation:

$$A_g = \frac{\lambda_g}{\lambda_g - \lambda_m} A_m^0 (e^{-\lambda_m t} - e^{-\lambda_g t}) + A_g^0 e^{-\lambda_g t}, \qquad (1)$$

where A_g is the specific activity of the sample at the cooling time t, while λ_g and λ_m are the decay constants for ground state and metastable isomer, respectively. The results were consistent (within 10%) with a direct measurement of 24.9 keV gamma line with a correction for intensity attenuation in the measured foil.

The experimental cross sections for population of the long-lived ^{57}Co nucleus ($T_{1/2}$=271.74 d) are based, following its decay, on the measurements of 122.06 KeV and 136.47 KeV γ-ray transitions of ^{57}Fe [68]. However, because the activation cross sections of ^{57}Co have been measured after more than 2 weeks from irradiation of the nickel target, they include also the contribution of ^{57}Ni ($T_{1/2}$=35.6 h) decay to ^{57}Co.

III. NUCLEAR MODEL ANALYSIS

A. Optical potential assessment

The simultaneous analysis of the deuteron elastic scattering and induced activation appears essential for a consistent input of nuclear model calculations [1–5] because the optical model potential (OMP) parameters which are obtained by the former data fit are then used within the calculation of all deuteron reaction cross sections. Because the Daehnick *et al.* [35] OMP was established on the basis of also the angular distributions of elastic scattered deuteron on $^{58,60-62,64}$Ni isotopes, it was a first option of the present analysis, too. The comparison of the experimental elastic-scattering angular distributions for $^{58,60-62,64}$Ni [20,36–42], at incident energies from ∼5 MeV towards 56 MeV, and the calculated values obtained by using this OMP and the computer code SCAT2 [46] is shown in the upper part of Fig. 1.

In the bottom part of the same figure the scarce systematics of measured total-reaction cross sections σ_R for the deuteron incident on ^{58,60,64}Ni isotopes [20,42–45] is compared with the calculated values corresponding to this OMP parameter, as well as the evaluated data within the TENDL-2015 library [17]. An overestimation of the only σ_R data around the incident energy of 40 MeV for ^{58}Ni target nucleus should be considered at the same time with the good agreement of the measured and calculated angular distributions at similar energies.

On the whole, the very good description of the measured elastic-scattering angular distributions and the suitable account of the available σ_R data supported well the OMP of Daehnick *et al.* for the further use in the calculation of deuteron interaction with Ni isotopes.

B. Deuteron breakup

1. Phenomenological approach

Because details concerning the physical picture of the deuteron breakup in the Coulomb and nuclear fields of the target nucleus were given more recently [5], only particular points are mentioned in the following. Two distinct processes

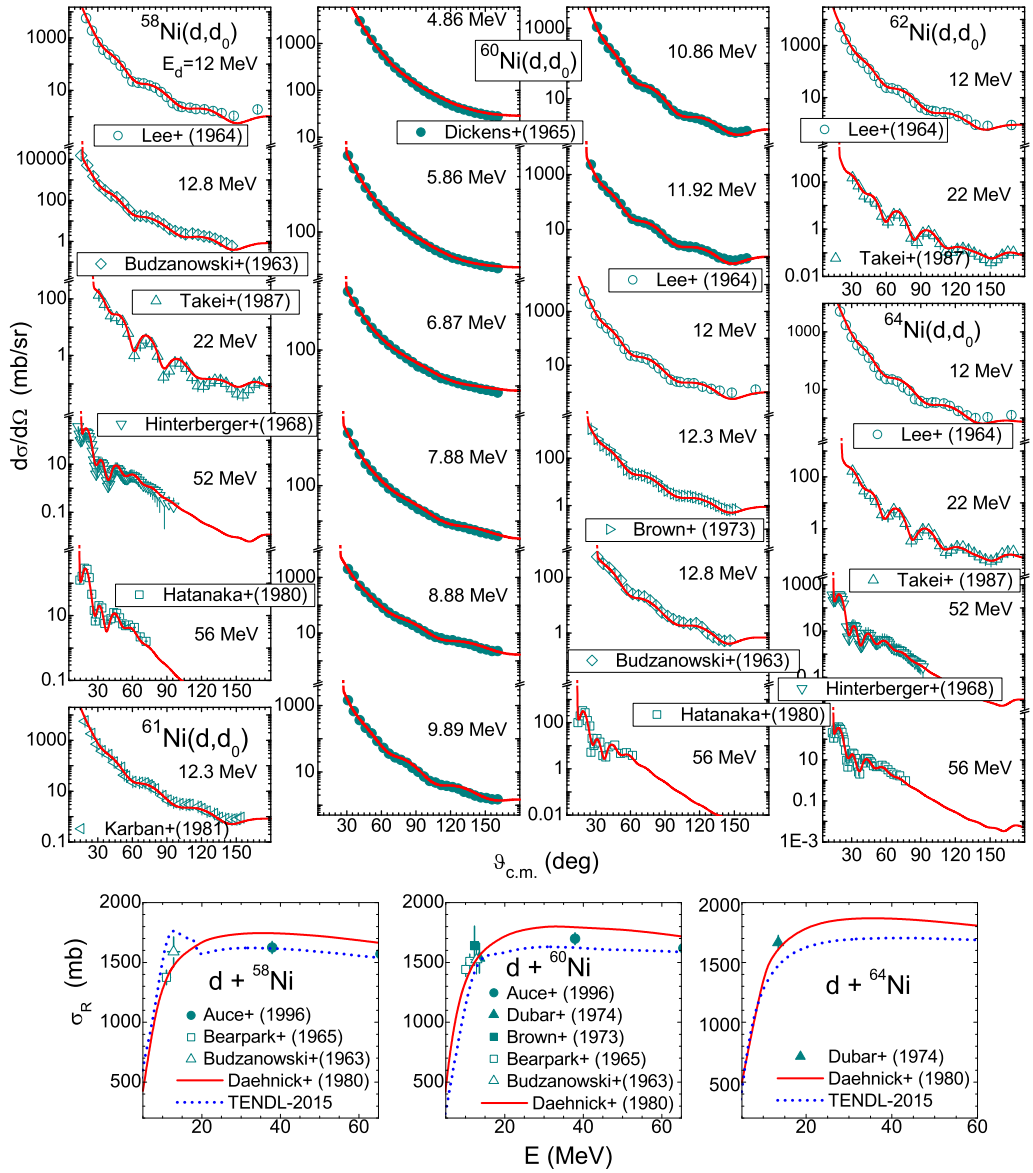

FIG. 1. (Top) Comparison of measured [20,36–42] and calculated elastic-scattering angular distributions of deuterons on $^{58,60-62,64}$Ni at energies from 5 to ∼60 MeV, using the global OMP of Daehnick *et al.* [35]; (bottom) comparison of measured [20,42–45], evaluated [17], and calculated total-reaction cross sections using the same OMP of deuterons on ^{58,60,64}Ni from 5 to ∼60 MeV.

are considered in this respect, namely the elastic breakup (EB) in which the target nucleus remains in its ground state and none of the deuteron constituents interacts with it, and the inelastic breakup or breakup fusion (BF), where one of these deuteron constituents interacts nonelastically with the target nucleus. The empirical parametrization [1,3,47] of both the elastic breakup (EB) and the total proton BU including also the inelastic breakup or breakup fusion (BF) has also been involved in the present work.

A comparison of predictions of this parametrization as well as of that of Kalbach [48] and the experimental [49–52] total (EB+BF) *proton*-emission breakup fractions $\sigma_{\rm BU}^{p}/\sigma_R$ for target nuclei from Al to Th is shown in Fig. 4 of Ref. [5]. Regardless the Kalbach high values at the lowest incident energies, the predictions of both parametrization within the energy range ∼10–60 MeV are close to each other, in a reasonable agreement with the experimental data. This is shown there to be also the case of the ^{58,62}Ni target nuclei, in support of the confidence in BU cross-section calculations within the present work. Nevertheless, the somewhat scarce experimental systematics of the deuteron BU data [49–53] may lead to large uncertainties of the BU cross-section energy dependence at deuteron energies over 60 MeV. These uncertainties can be decreased only by means of new experimental breakup data.

The similar agreement between Kalbach [48] and Avrigeanu *et al.* [1,3,47] parametrizations, except the deuteron incident energies lower than ∼10 MeV, is found for the total proton-emission BU cross sections for deuteron interactions

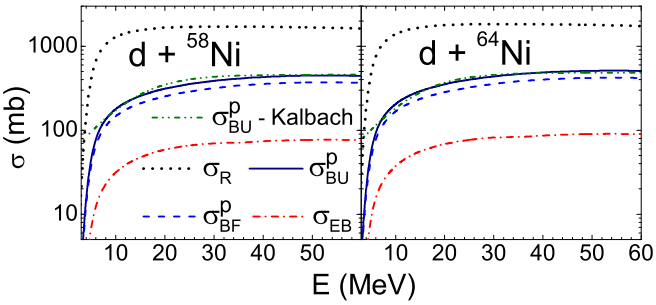

FIG. 2. The energy dependence of the deuteron total-reaction cross sections [35] (dotted curves), total proton-emission breakup cross sections given by parametrizations of Refs. [48] (dash-dot-dotted curves) and [1] (solid curves), and EB (dash-dotted curves) and BF (dashed curves) breakup components [1], for deuteron interactions with ^{58,64}Ni.

with $^{58,60-62,64}$Ni, and shown in Fig. 2 for ^{58,64}Ni isotopes. Thus, the corresponding comparison of the deuteron total-reaction cross section and total BU proton-emission excitation functions underlines the importance of the breakup mechanism for deuteron interacting with Ni isotopes. Moreover, the excitation functions of the BF and the EB components, which are also shown in Fig. 2 as given specifically by Avrigeanu *et al.* parametrization, have a particular meaning for the BU contribution to various activation cross sections.

2. *Inelastic breakup enhancement*

The above-mentioned BF dominance over the much weaker EB component emphasizes the latter of the two opposite effects of the deuteron breakup on the deuteron activation cross sections. Thus, while first the total-reaction cross section, that is shared among different outgoing channels, is reduced by the value of the total neutron and proton breakup cross section $\sigma_{\rm BU}$ [1,3,47], the BF component may bring significant contributions to various reaction channels [2–5,54–56]. So, the absorbed proton or neutron following the deuteron breakup, contributes to the enhancement of the corresponding (d,xn) or (d,xp) activation cross sections, respectively. On the other hand it should be underlined that the reactions induced by BF nucleons are related to the deuteron BU process because they are just subsequent to this one, while they proceed through different compound nuclei than the incident deuteron do.

The partition of the BF cross section among various residual nuclei is triggered by the energy spectra of the BF nucleons and the excitation functions of the CN reactions induced by these nucleons on the target nuclei [2–5,54]. Thus, to calculate the BF enhancement of, e.g., the (d,xn) reaction cross sections, the BF proton-emission cross section $\sigma^p_{\rm BF}$ should be (i) multiplied by the ratios $\sigma_{(p,x)}/\sigma^p_R$, corresponding to the above-mentioned enhancing reaction, (ii) convoluted with the Gaussian line shape distribution of the BF proton energy E_p for a given deuteron incident energy E, and followed by (iii) an integration over the BF proton energy. Consequently, the BF enhancement cross section has the form [5,55,56]:

$$\sigma^{p,x}_{\rm BF}(E) = \sigma^p_{\rm BF}(E) \int dE_p \ \frac{\sigma_{(p,x)}(E_p)}{\sigma^p_R} \times \frac{1}{(2\pi)^{\frac{1}{2}} w} \exp\left[- \frac{\left(E_p - E^0_p(E)\right)^2}{2w^2} \right], \quad (2)$$

where σ^p_R is the proton total-reaction cross section, x stands for various, e.g., γ, n, d, or α outgoing channels, while E^0_p and w are the centroid and standard deviation, respectively, of the above-mentioned BU proton-energy Gaussian distribution given by Kalbach [48] related parameters. Interpolation of experimental nucleon-induced reaction cross sections from the EXFOR library [57] was involved within this estimation of the BU enhancement [2–5,54–56] to reduce as much as possible the supplementary uncertainties brought by additional theoretical calculations. These neutron and proton EXFOR data are replaced by the TENDL-2015 evaluated excitation functions within a BU enhancement inclusion in TALYS-1.8 which is currently under development.

Last but not least, with reference to the integration over the BF proton energy, one may note that the excitation energies of the CNs which are formed by the incident deuteron and the BF nucleons, respectively, are quite different.

The BF enhancements from the BU protons and neutrons emitted during the deuteron interaction with ^{nat}Ni through the (p,γ), (p,n), (p,α), $(p,2n)$, $(p,2p)$, $(p,\alpha n)$, $(p,2\alpha)$, $(p,3n)$, $(p,2pn)$, (n,γ), (n,d), (n,α), $(n,\alpha p)$, $(n,2\alpha)$, $(n,2n)$, $(n,2np)$ reactions populating various residual nuclei, are discussed in Sec. IV (Figs. 7–22).

C. Direct reactions

The interactions of deuterons with medium-mass target nuclei at energies around the Coulomb barrier proceed largely through the DR mechanism [7] which is therefore quite important for the cross sections related to the first-chance emitted particle (d,p), (d,n), (d,t), and (d,α) residual channels. Thus, the assessment of the total transfer reaction cross section is mandatory, in spite of very poor attention or even not accounted so far in deuteron activation analysis. Unfortunately, it is conditioned by the available experimental spectroscopic factors or at least outgoing particle angular distributions. Nevertheless, similarly to the breakup mechanism, we have to take into account also the decrease the deuteron flux going towards statistical processes, corresponding to the transfer reactions that enhance the first-chance emission particle reactions.

The appropriate calculation of the DR stripping and pick-up mechanism contributions was performed using the distorted-wave Born approximation (DWBA) method within the highly developed coupled-reaction channels (CRC) formalism and the advanced code FRESCO [15]. The post- or prior form distorted-wave transition amplitudes for $(d,n/p)$ stripping and, respectively, $(d,t/\alpha)$ pick-up reactions, and the finite-range interaction have been considered. The n-p effective interaction in deuteron [58] as well as d-n effective interaction in triton [59] were assumed to have a Gaussian shape, at the same time with a Woods-Saxon shape [60] of the d-d effective interaction in the α particle. The transferred nucleon

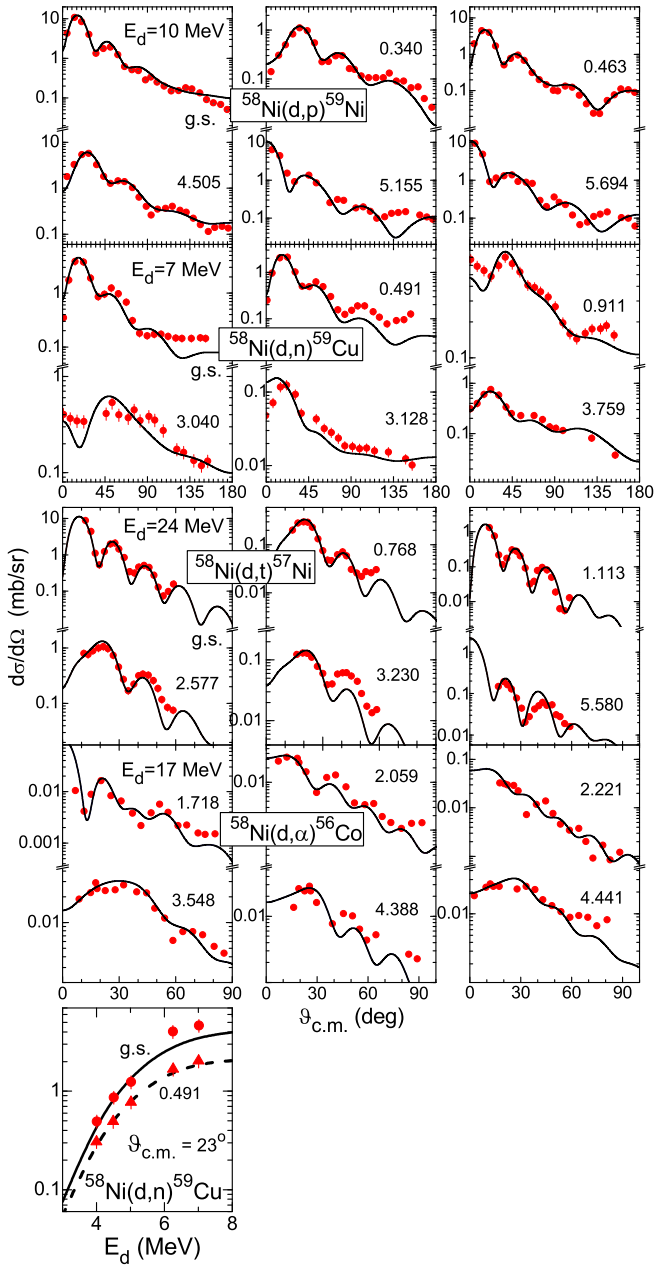

FIG. 3. Comparison of calculated (solid curves) and measured proton [71], neutron [72], triton [73], and α-particle [74] angular distributions, for (d,p) and (d,n) stripping, and (d,t) and (d,α) pick-up transitions to states with excitation energies in MeV, and deuterons on ^{58}Ni at energies between 7 and 24 MeV, and (bottom) measured [72] and calculated excitation functions from 3 to 8 MeV of differential cross sections of ^{58}Ni$(d,n)^{59}$Cu transitions to the ground (g.s.) and first excited states, at $\theta_{\text{c.m.}}$=23°.

and deuteron bound states were generated in a Woods-Saxon real potential [1,3–5,55,56] while the transfer of the deuteron cluster was taken into account for the (d,α) pick-up cross-section calculation. The populated discrete levels and the corresponding spectroscopic factors which have been available within the ENSDF library [61] were used for the (d,n) and (d,p) stripping [62–66], and (d,t) and (d,α) pick-up processes [62–65,67–70].

The suitable description of the experimental proton [71], neutron [72], triton [73], and α-particle [74] angular distributions, for (d,p) and (d,n) stripping, and (d,t) and (d,α) pick-up transitions, respectively, to states of the corresponding residual nuclei, was standing for the validation of the spectroscopic information used and the finally calculated total stripping and pick-up reaction cross sections. An illustration for the complete analysis of the DR contributions for deuteron interaction with ^{58}Ni is shown in Fig. 3. Additionally, a comparison of the measured [72] and calculated excitation functions from 3 to 8 MeV of differential cross sections of ^{58}Ni$(d,n)^{59}$Cu stripping transitions to the ground (g.s.) and first excited states, at $\theta_{\text{c.m.}}$=23°, is also shown there. Finally on this point, the calculated excitation functions for stripping and pick-up processes induced by deuterons on the ^{58}Ni target is shown within the systematics of Ni isotopes in Fig. 6.

The particularly strong (d,p) stripping processes, being also of critical importance for the nuclear structure studies, have the advantage of a reliable systematics of the experimental spectroscopic factors extracted from the analysis of experimental proton angular distributions which did contribute to the validation of the nuclear shell model. Consequently, it was possible the calculation of almost total (d,p) stripping cross-section contributions to the deuteron activation for $^{58,60-62,64}$Ni isotopes, involving, e.g., population of 65 levels

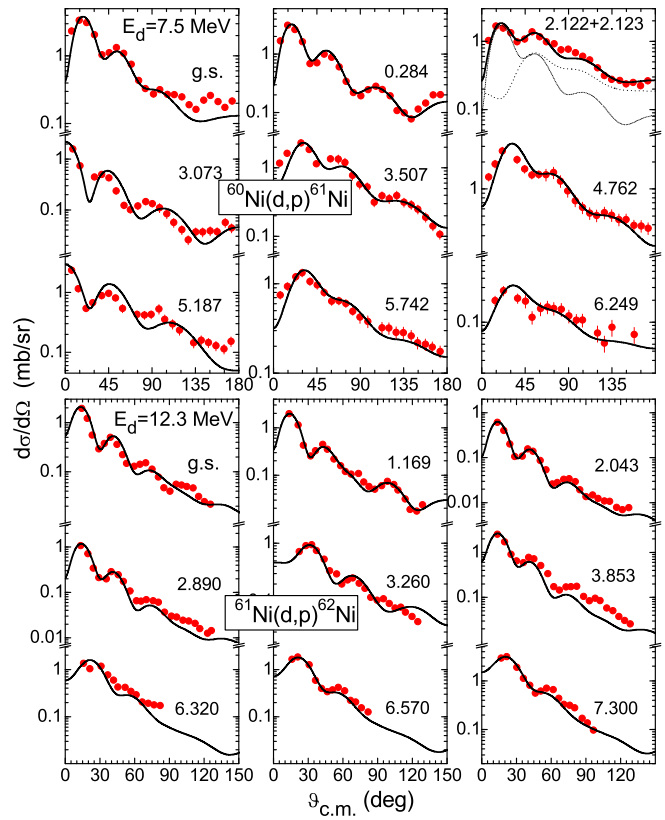

FIG. 4. Comparison of measured [40,75] and present calculation (solid curves) of proton angular distributions of ^{60}Ni$(d,p)^{61}$Ni and ^{61}Ni$(d,p)^{62}$Ni transitions to the shown states of the residual nuclei, at incident energies of 7.5 MeV and 12.3 MeV, respectively.

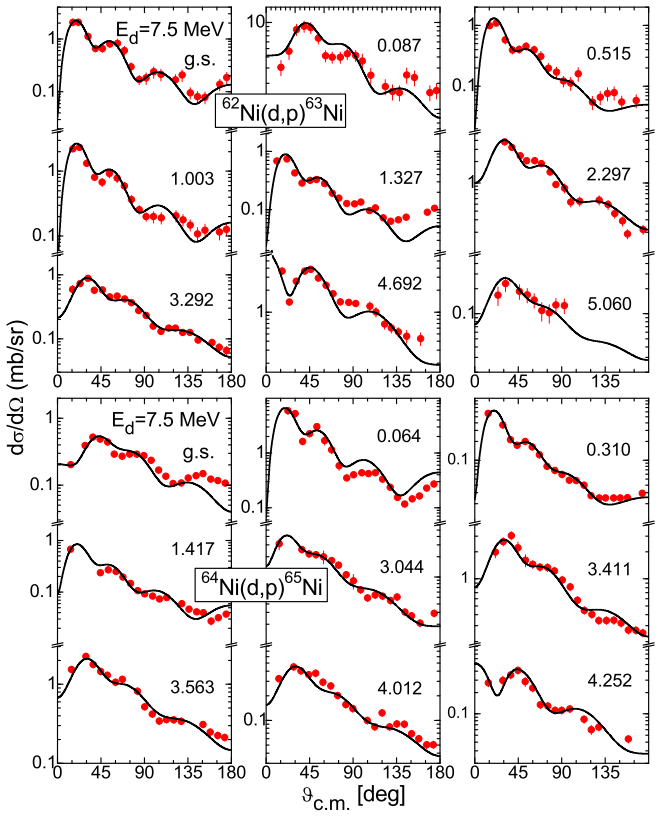

FIG. 5. As Fig. 4 but for ^{62}Ni$(d,p)^{63}$Ni and ^{64}Ni$(d,p)^{65}$Ni stripping reactions at the incident energy of 7.5 MeV [76].

in ^{59}Ni [62], 91 levels in ^{61}Ni [63], 31 levels in ^{62}Ni [64], 52 levels in ^{63}Ni [65], and 45 levels in ^{65}Ni [66] corresponding residual nuclei. A comparative analysis of the experimental [40,71,75,76] and calculated angular distributions of the stripped protons from the (d,p) transfer reactions on $^{60-62,64}$Ni isotopes is shown in Figs. 4 and 5. The appropriate description of the measured data gives the confidence in the correctness of the theoretical stripping excitation functions shown in the lower part of Fig. 6.

On the contrary, the experimental neutron, triton, and α-particle angular distributions as well as spectroscopic factors for stripping (d,n) and pick-up (d,t) and (d,α) reactions on Ni isotopes are scarce. Therefore, the corresponding cross sections, e.g., of the ^{61}Ni(d,n)^{62}Cu, ^{61}Ni$(d,\alpha)^{59}$Co, ^{64}Ni$(d,\alpha)^{62}$Co reactions, cannot be accurately estimated or at best could be underestimated. The calculated excitation functions for the stripping and pick-up reactions induced by deuterons on $^{58,60-62,64}$Ni isotopes are conclusively shown in the bottom of Fig. 6.

Following the discussion of the BU and DR processes, i.e., the direct interactions (DI) of deuterons with Ni isotopes, it is worthwhile to have an overview of the deuteron flux which remains available for PE and fully equilibrated CN decay. It can be given by a reduction factor of the total-reaction cross section because of the cross sections of the various DI components:

$$1-\frac{\sigma_{\rm BU}+\sigma_{(d,n)}+\sigma_{(d,p)}+\sigma_{(d,t)}+\sigma_{(d,\alpha)}}{\sigma_R}=1-\frac{\sigma_{\rm DI}}{\sigma_R}. \quad (3)$$

Its energy dependence is shown for $^{58,60-62,64}$Ni isotopes in Fig. 6 at the same time with that of the BU, stripping, and pick-up reactions. Thus, one may note first a steep increase with energy of this reduction factor since the major BU but also and especially the DR components increase with energy. Most significant in this respect is the maximum of the (d,p) and (d,n) stripping excitation functions around 6–8 MeV, which provides the fastest slope of this factor. A less steep increase with the energy corresponds to the reduction factor for the ^{61}Ni target nucleus, because the lack of information concerning the (d,n) and (d,α) reactions is followed by an obvious underestimation of the DI cross section. Then, the reduction factor reaches its own maximum and continues with a slow decrease because of a slower increase with energy of the BU+DR excitation functions than σ_R, for all Ni isotopes. Thus, the remaining deuteron total-reaction cross section for the PE+CN statistical processes is slightly increasing above the deuteron energies of 15–20 MeV but close to only half of the OMP values.

The significant effects of the stripping (d,p), (d,n), and pick-up (d,t) reactions for the deuteron interaction with Ni

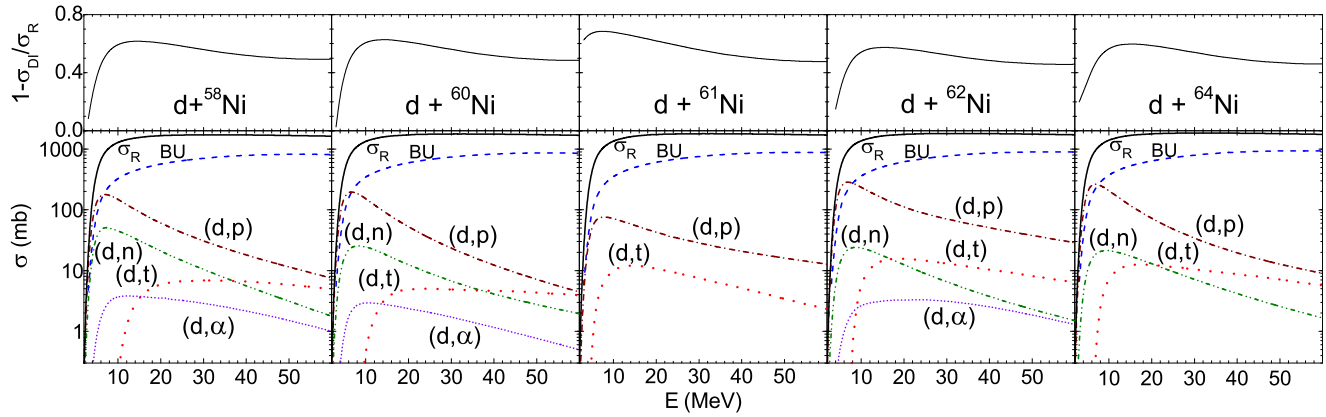

FIG. 6. (Bottom) Total-reaction (solid curves), BU (dashed curves), stripping (d,n) (dash-dot-dotted curves) and (d,p) (dash-dotted curves), and pick-up (d,t) (dotted curves) and (d,α) (short-dotted curves) reaction cross sections for deuterons on $^{58,60-62,64}$Ni, and (top) the corresponding reduction factors of the deuteron flux going towards statistical processes (solid curves).

isotopes have been summed up in Figs. 7, 8, and 11. Less important, the pick-up (d,α) mechanism contribution is shown in Figs. 14, 15, 16, and 18.

D. Statistical emission

The PE and CN statistical processes become important with the increase of the incident energy above the Coulomb barrier (e.g., Ref. [7]). The corresponding reaction cross sections have been calculated using the TALYS-1.8 code [16] and the reduction factor of Eq. (3) to take into account the above-mentioned breakup, stripping, and pick-up results.

The following input options of the TALYS-1.8 code have been used: (a) the OMPs of Koning-Delaroche [77], Daehnick *et al.* [35], Becchetti-Greenlees [78], and Avrigeanu *et al.* [79], for neutrons, protons, deuterons, tritons, and α particles, respectively; (b) the back-shifted Fermi gas (BSFG) formula for the nuclear level density; (c) no TALYS breakup contribution, because the above-mentioned BF enhancements are still under implementation in TALYS; (d) the PE transition rates calculated by means of the corresponding OMP parameters, using the value 3 for the "preeqmode" keyword of TALYS.

IV. RESULTS AND DISCUSSION

The detailed contributions of various Ni isotopes to the excitation function for the activation of a certain residual nucleus by deuteron interaction with ^{nat}Ni are compared in Figs. 7–22 with the measured cross sections of Sec. II and formerly available [8–10,20–33] as well as with the TENDL-2015 predictions [17]. While some PE+CN contributions are not shown for all Ni stable isotopes in Figs. 7–22, they were all considered within the cross-section calculation for natural Ni. A global comparison of the data and calculated results for ^{nat}Ni is shown in Fig. 23. The proper description of the reaction mechanisms that have been considered in the present work is proved by the overall agreement of experimental and calculated excitation function. Additionally, particular comments should concern several reaction categories as follows. We shall refer first to the heavier residual nuclei because fewer stable isotopes of Ni have been involved for their population, while more isotopes, processes, and emitted particles are involved in the case of the lighter products.

A. The (d,p) reaction

The analysis of the population of ^{65}Ni residual nucleus through the deuteron interaction with ^{nat}Ni target involves actually only the deuteron interaction with the neutron-richest ^{64}Ni stable isotope. Moreover, a suitable account of the ^{64}Ni$(d,p)^{65}$Ni reaction represents in particular a distinct test of the reaction model approach from the dominant contribution of the stripping DR mechanism whose consideration is critical for the suitable account of the measured cross sections. On the other hand, the corresponding activation data, which were measured in the present work for the natural nickel, have been most useful to cross out an apparent discontinuity at an incident energy of 7–8 MeV within the only excitation function measured previously for ^{64}Ni isotope (Fig. 7).

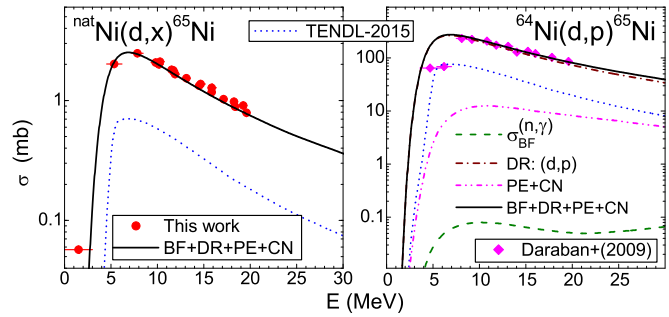

FIG. 7. Comparison of previous [21] and present (solid circles) measurements, TENDL-2015 [17] evaluation (dotted curves), and present calculation (solid curves) of ^{64}Ni$(d,p)^{65}$Ni and ^{nat}Ni$(d,x)^{65}$Ni reaction cross sections, along with BF enhancement (dashed curve), stripping (d,p) reaction (dash-dotted curve), and PE+CN components (dash-dot-dotted curve) corrected for DI deuteron flux leakage.

The comparative analysis of the contributions of all reaction mechanisms involved in the ^{64}Ni$(d,p)^{65}$Ni reaction (Fig. 7) shows that the PE+CN contribution to the population of ^{65}Ni residual nucleus is more than of order magnitude lower than the stripping one, while the inelastic breakup enhancement brought by breakup neutrons through the ^{64}Ni$(n,\gamma)^{65}$Ni reaction is practically negligible in this case. The effect of neglecting the key role of the direct stripping process is illustrated by the strong underestimation of both experimental ^{64}Ni$(d,p)^{65}$Ni [21] and ^{nat}Ni$(d,p)^{65}$Ni reaction excitation functions by TENDL-2015 evaluation. Actually, this proof is just in line with the previous discussion of the experimental (d,p) excitation functions for ^{58}Fe [5] and ^{93}Nb [4] target nuclei, which cannot be described as long as the strong stripping contribution is neglected.

B. (d,xn) reactions and ^{60,61,64}Cu residual nuclei population

The (d,n) stripping process is less spectacular than the (d,p) one, as it can be seen also from the bottom of Fig. 6. However, its role is particularly obvious within the analysis of the experimental cross sections of both ^{60}Ni$(d,n)^{61}$Cu [20,25,26] and ^{nat}Ni$(d,x)^{61}$Cu [8,10,22–24] reactions (Fig. 8). These data would be underestimated if the stripping DR contribution, even larger than the whole TENDL-2015 evaluation above 20 MeV, is not properly taken into account.

Actually the model calculations including contributions from BU, stripping, and PE+CN mechanisms describe the experimental ^{60}Ni$(d,n)^{61}$Cu excitation function [20,26] except its maximum measured earlier [25], for deuteron energies of 5.5–12 MeV, at variance with the data for the Ni element reported previously [8,10,22–24] (Fig. 8) and confirmed by the present work. Weighty contributions to the population of ^{61}Cu residual nucleus comes also from the $(d,2n)$ and $(d,3n)$ reactions on ^{61,62}Ni isotopes, respectively, where the BF processes through ^{61}Ni(p,n) and ^{62}Ni$(p,2n)$ reactions go over the statistical PE+CN mechanisms at deuteron energies higher than ∼25 MeV. The decrease of the (d,xn) excitation function becomes thus much slower within this energy range, comparing to its steep increase above the threshold. In fact, it

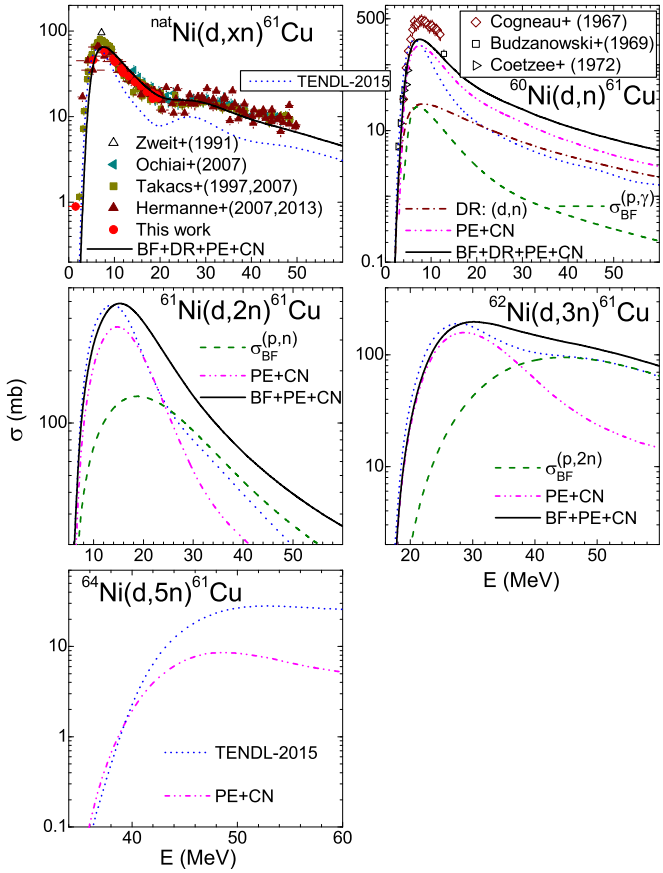

FIG. 8. Comparison of previous [8,10,20,22–26] and present (solid circles) measurements, TENDL-2015 [17] evaluation (dotted curves), and present calculation (solid curves) of ^{nat}Ni(d,xn)^{61}Cu, ^{60}Ni(d,n)^{61}Cu, ^{61}Ni(d,$2n$)^{61}Cu, ^{62}Ni(d,$3n$)^{61}Cu, and ^{64}Ni(d,$5n$)^{61}Cu reaction cross sections, along with BF enhancement (dashed curves), stripping (d,n) reaction (dash-dotted curve), and PE+CN components (dash-dot-dotted curves) corrected for DI deuteron flux leakage.

is worth noticing the significant BF contribution to the second and third sequential particle emission in the deuteron-induced reaction, while the DR stripping and pick-up contributions play the same role for the first-chance emitted particles.

The same decrease of the PE+CN importance versus that of the BF mechanism at deuteron energies higher than ∼25 MeV occurs also for the population of ^{64}Cu residual nucleus through the (d,$2n$) reaction on ^{64}Ni (Fig. 9). The decrease of the calculated excitation function, which is slower than, e.g., in the case of the TENDL-2015 evaluation, follows just the BF enhancement from the BU protons and the corresponding ^{64}Ni(p,n)^{64}Cu reaction. Additionally, it could be pointed out the similar cases of the residual nuclei ^{65}Ni (Fig. 7) and ^{64}Cu (Fig. 9), populated in deuteron interactions with the natural Ni through the activation of only one isotope of this element, except the major role of the DR, for the former, and BF processes for the latter.

The similar (d,$2n$) reaction on the ^{60}Ni isotope is dominant for the population of ^{60}Cu (Fig. 10). The larger part of this contribution comes again from the BU protons through

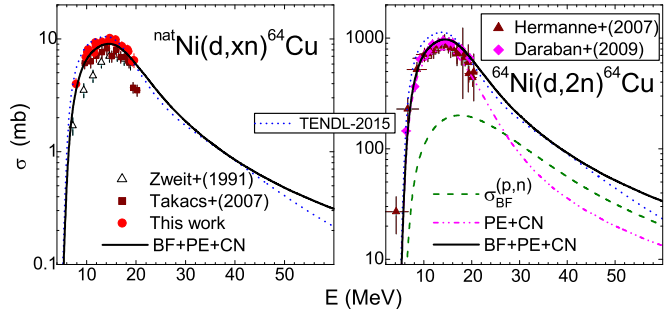

FIG. 9. As Fig. 7 but for ^{nat}Ni(d,xn)^{64}Cu [10,22] and ^{64}Ni(d,$2n$)^{64}Cu [8,21] reactions, and no stripping component.

the ^{60}Ni(p,n)^{60}Cu reaction, leading to a slower decrease of the corresponding excitation functions. On the other hand, the cross sections measured in the present work for the ^{nat}Ni(d,x)^{60}Cu reaction do confirm at once the previous data [23,24] as well as the presently calculated values, while the earlier measurement [27] for the ^{60}Ni(d,x)^{60}Cu reaction is at variance with the present calculations as well as the TENDL-2015 evaluation. A comment may concern the contributions from the ^{61,62,64}Ni isotopes through emission of 3–6 neutrons, respectively, which are much lower.

C. The (d,t) reaction and ^{56,57}Ni residual nuclei population

The (d,t) pick-up contribution to a total (d,x) activation cross section, which is usually neglected in deuteron activation calculations, is also noteworthy. It is responsible for the low-energy side of the excitation function, namely at the energies below the (d,dn) and (d,$p2n$) reaction thresholds which end by population of the same residual nucleus. This is the case of the ^{nat}Ni(d,x)^{57}Ni and ^{58}Ni(d,x)^{57}Ni reaction

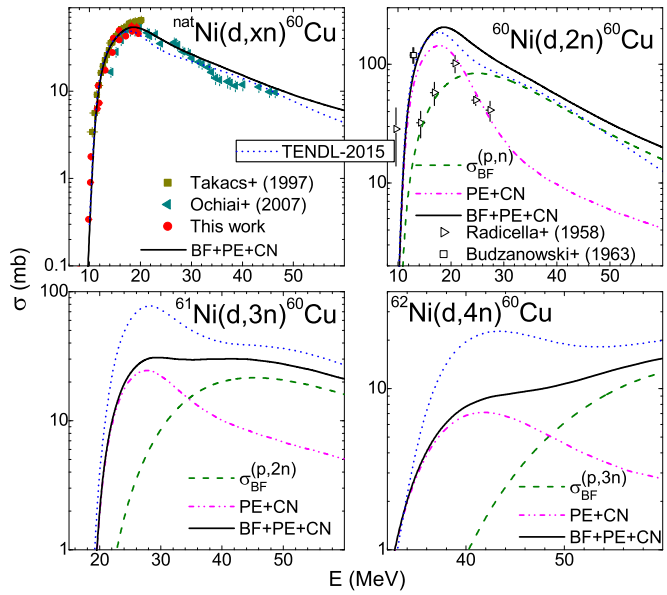

FIG. 10. As Fig. 9 but for ^{nat}Ni(d,xn)^{60}Cu [10,23], ^{60}Ni(d,$2n$)^{60}Cu [20,27], ^{61}Ni(d,$3n$)^{60}Cu, and ^{62}Ni(d,$4n$)^{60}Cu reactions.

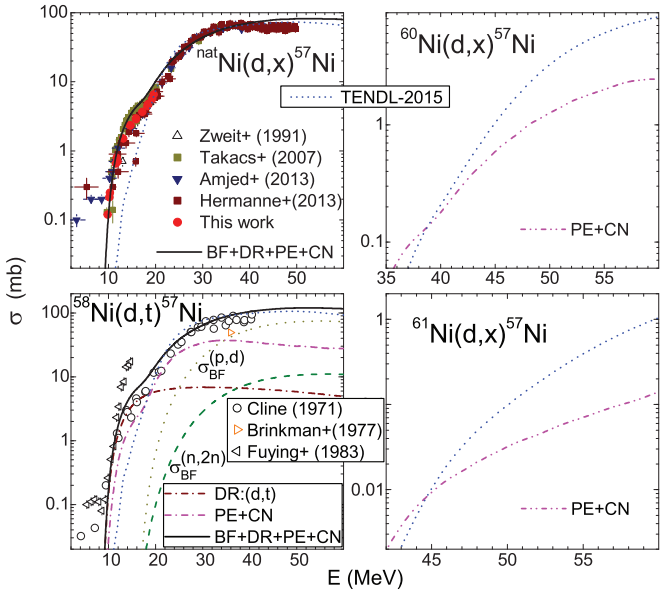

FIG. 11. Comparison of previous [8–10,22,28–30] and present (solid circles) measurements, TENDL-2015 [17] evaluation (short-dotted curves), and present calculation (solid curves) of cross sections for ^{nat}Ni$(d,x)^{57}$Ni, ^{58}Ni$(d,x)^{57}$Ni, ^{60}Ni$(d,x)^{57}$Ni, and ^{61}Ni$(d,x)^{57}$Ni reactions, BF enhancement (dashed and dotted curves), pick-up (d,t) reaction (dash-dotted curve), and PE+CN components (dash-dot-dotted curves) corrected for DI deuteron flux leakage.

excitation functions (Fig. 11), the presently measured cross sections for the former reaction characterizing more accurately the energy region just above the (d,t) reaction threshold. On the other hand, the activation of ^{57}Ni residual nucleus is strongly enhanced by the BU neutrons as well as protons which interact with the ^{58}Ni target nucleus through ^{58}Ni$(n,2n)^{57}$Ni and ^{58}Ni$(p,d)^{57}$Ni reactions, respectively. The suitable description of the data for both of these excitation functions validates the theoretical approach of the deuteron interaction process. Moreover, the underestimation of their low-energy part by the latest evaluation TENDL-2015 could be just the effect of a less suitable account of the (d,t) pick-up process.

The lower cross sections for the population of the ^{56}Ni residual nucleus in deuteron interaction with ^{58,nat}Ni targets have been described only by means of the statistical PE+CN processes (Fig. 12), next to the correction for the initial deuteron flux leakage through direct interactions. Because no other BU or DR effects are present in this case, the better agreement of the present calculated results and the measured data, with reference to the TENDL-2015 evaluation, stands for an additional check for the accuracy of this correction.

D. The $(d,2p)$ and $(d,\alpha x)$ reactions

The $(d,2p)$ reaction is most important one for the population of the heavier ^{58,60,61}Co isotopes in the deuteron-induced reactions on natural nickel (Figs. 13–16). First, it is obvious the usefulness of the new measured data for the production of $^{56-58,60}$Co residual nuclei and particularly the ^{58}Co^{m} isomer.

Second, it should be pointed out here that a significant contribution of the inelastic breakup is added, through (n,p) reaction, to the PE+CN components of the $(d,2p)$ reaction corrected for the incident deuteron flux leakage due DI. Thus, the BF and PE+CN cross sections are almost equal or close at 60 MeV in the cases of the residual nuclei ^{61}Co (Fig. 13) and ^{58}Co (Figs. 15 and 16), respectively. Particularly, the BF starts to be larger even from ∼30 MeV for ^{60}Co (Fig. 14). The increase of the corresponding cross sections and their agreement with the experimental data, including the measurements within this work, stand for a sound proof of the present careful consideration of the BU and DR mechanisms. One may note in this respect the larger calculated results, with reference to the TENDL-2015 evaluation, in good agreement with the recent data [10] of the reaction ^{nat}Ni$(d,x)^{61}$Co (Fig. 13). A worthwhile note concerning Ref. [10] may concern the only problem of the measured cross sections for the reaction ^{nat}Ni$(d,x)^{60}$Co, being evident also in Fig. 14, which was clarified recently [8].

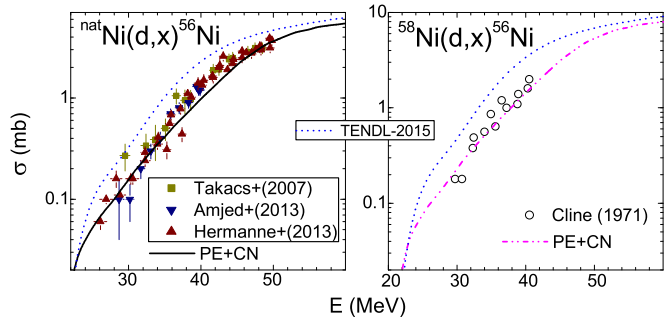

FIG. 12. As Fig. 7 but for ^{nat}Ni$(d,x)^{56}$Ni [8–10] and ^{58}Ni$(d,x)^{56}$Ni [28] reactions, and no DI component.

The BF contribution has also become equal, at higher incident energies, to the PE+CN components for population of the lighter ^{55,56,57}Co residual nuclei. A particular point of

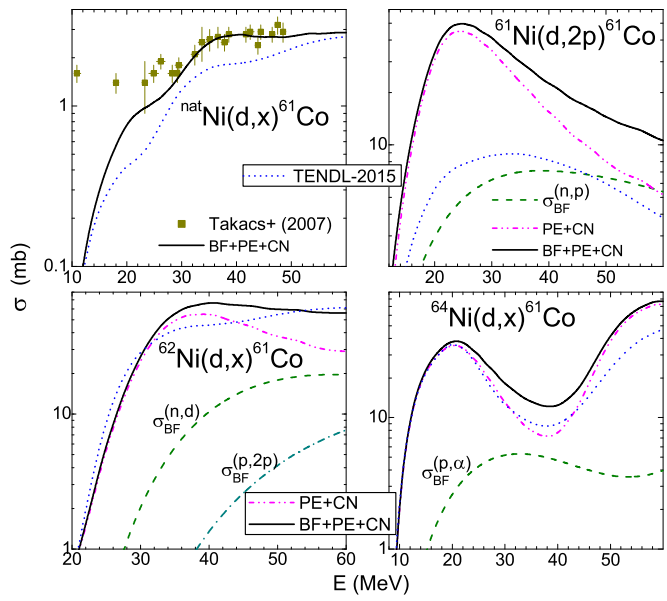

FIG. 13. As Fig. 9 but for ^{nat}Ni$(d,x)^{61}$Co [10], ^{61}Ni$(d,2p)^{61}$Co, ^{62}Ni$(d,x)^{61}$Co, and ^{64}Ni$(d,x)^{61}$Co reactions.

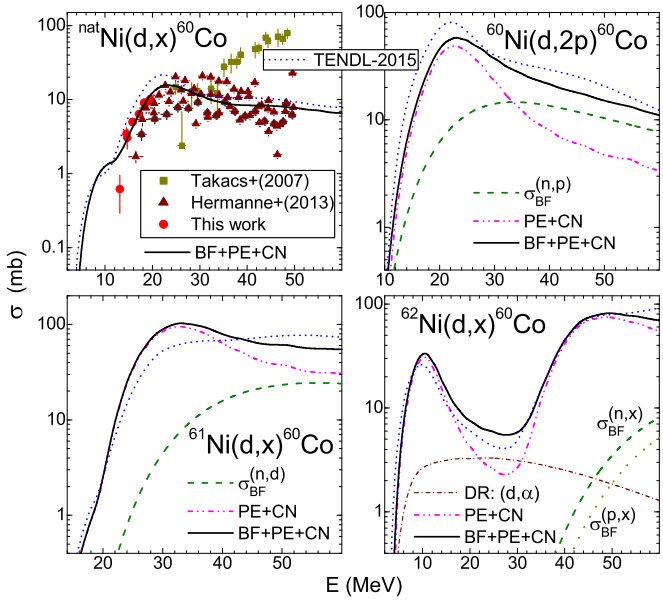

FIG. 14. As Fig. 9 but for ^{nat}Ni$(d,x)^{60}$Co [8,10], ^{60}Ni$(d,2p)^{60}$Co, ^{61}Ni$(d,x)^{60}$Co, and ^{62}Ni$(d,x)^{60}$Co reactions, and pick-up (d,α) reaction (dash-dotted curve).

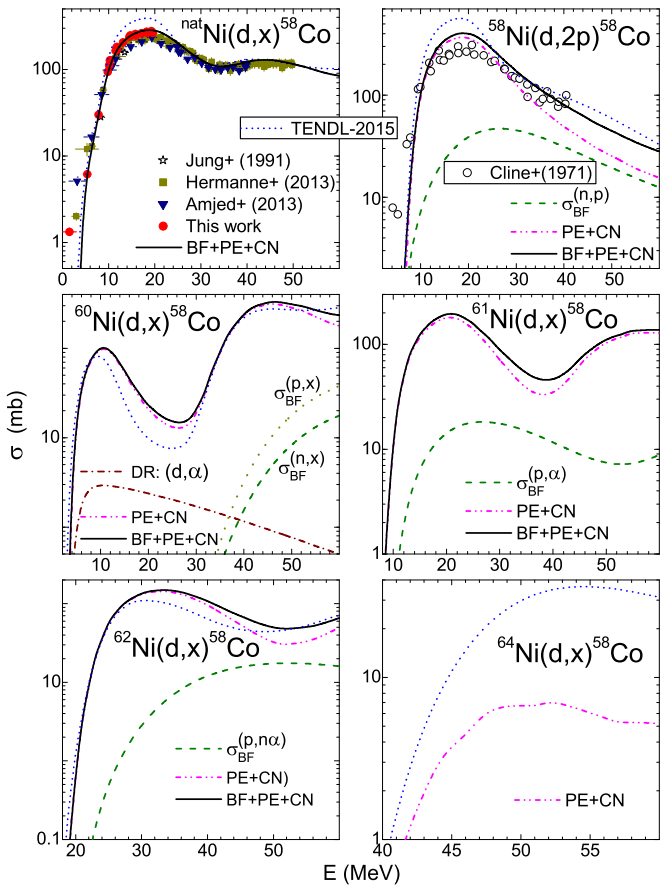

FIG. 15. As Fig. 14 but for ^{nat}Ni$(d,x)^{58}$Co [8,9,31], ^{58}Ni$(d,2p)^{58}$Co [28], ^{60}Ni$(d,x)^{58}$Co, ^{61}Ni$(d,x)^{58}$Co, ^{62}Ni$(d,x)^{58}$Co, and ^{64}Ni$(d,x)^{58}$Co reactions.

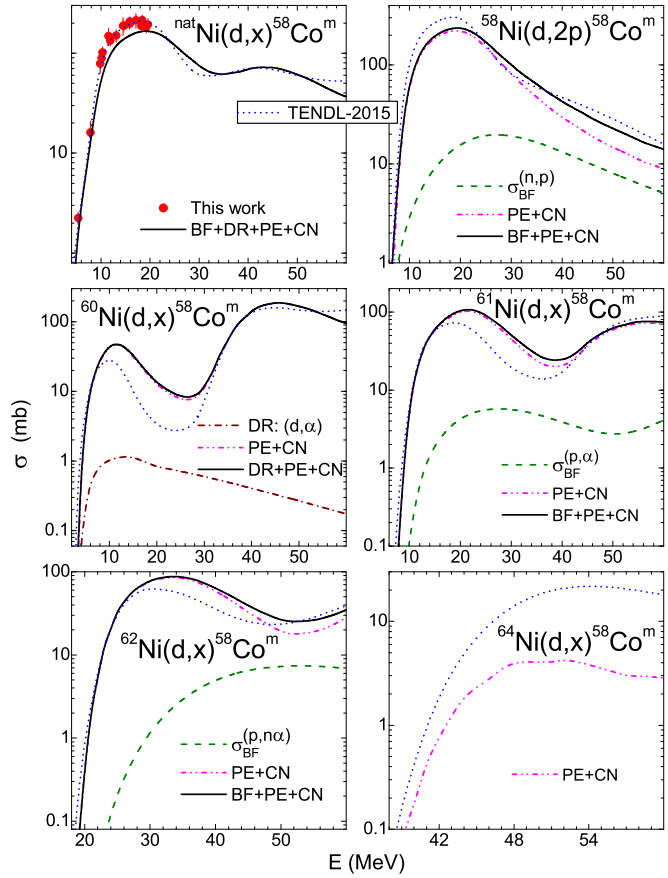

FIG. 16. As Fig. 14 but for ^{nat}Ni$(d,x)^{58}$Co^{m}, ^{58}Ni$(d,2p)^{58}$Co^{m}, ^{60}Ni$(d,x)^{58}$Co^{m}, ^{61}Ni$(d,x)^{58}$Co^{m}, ^{62}Ni$(d,x)^{58}$Co^{m}, and ^{64}Ni$(d,x)^{58}$Co^{m} reactions.

the excitation functions measured for the ^{nat}Ni$(d,x)^{56,57}$Co reactions, above mentioned in Sec. II, has concerned the cumulative populations of ^{56,57}Co residual nuclei. Therefore, the measured data had to be compared to the sum of the cross sections for ^{nat}Ni$(d,x)^{57}$Co and ^{nat}Ni$(d,x)^{57}$Ni reactions (denoted by the superscript + in Fig. 17).

Similarly, the reported experimental activation cross sections of long-lived ^{56}Co residual nucleus ($T_{1/2}$ = 77.24 days), based on the measurements of 846.77 KeV, 1037.84 KeV, and 1238.29 KeV γ-ray transitions of ^{56}Fe [67], include the contribution of ^{56}Ni ($T_{1/2}$ = 6.075 days) decay, too. The measured data had to be compared to the sum of the cross sections for ^{nat}Ni$(d,x)^{56}$Co and ^{nat}Ni$(d,x)^{56}$Ni reactions for incident energies above 20 MeV (Fig. 18).

Therefore, the experimental data for the populations of ^{56,57}Co residual nuclei have been compared in Figs. 18 and 17, respectively, with the cumulative calculated and evaluated excitation functions for ^{nat}Ni$(d,x)^{56,57}$Co^{+} reactions which include the contributions of ^{nat}Ni$(d,x)^{56,57}$Ni reactions which were already shown in Figs. 12 and 11. Also shown in Figs. 18 and 17, respectively, are the results for the stand-alone reactions ^{58}Ni$(d,x)^{56,57}$Co and ^{60}Ni$(d,x)^{56,57}$Co, on the main ^{58,60}Ni isotopes, with the twofold aim to illustrate the reaction mechanisms contributing to their own populations of ^{56,57}Co residual nuclei, and the effect of their cumulative population.

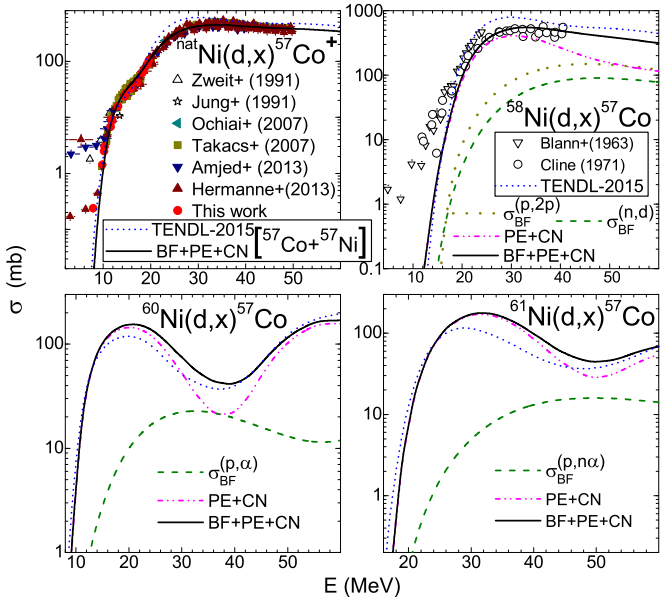

FIG. 17. As Fig. 9 but for ^{nat}Ni$(d,x)^{57}$Co [8–10,22–24,31] including the decay of ^{57}Ni, ^{58}Ni$(d,x)^{57}$Co [28,32], ^{60}Ni$(d,x)^{57}$Co, and ^{61}Ni$(d,x)^{57}$Co reactions.

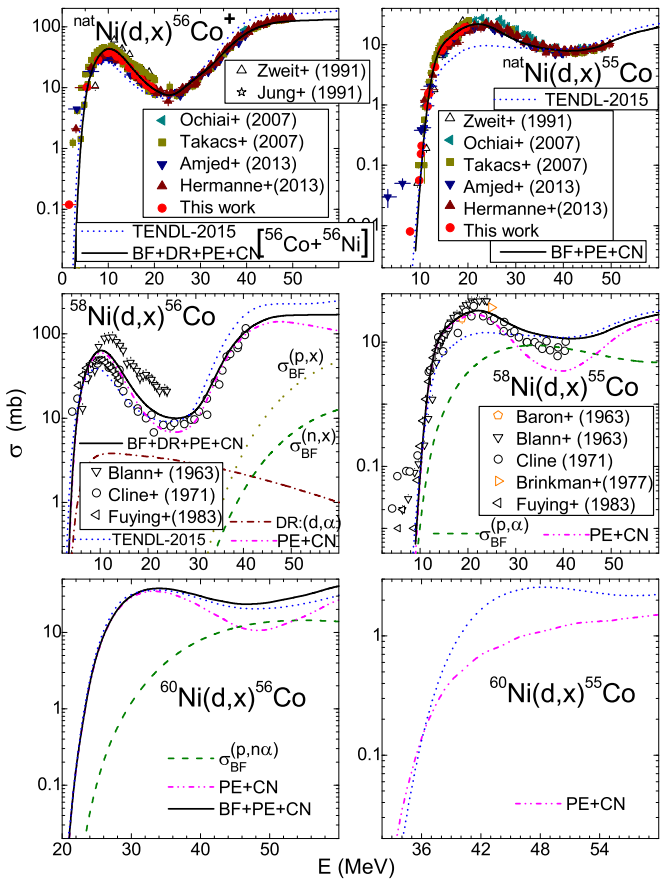

FIG. 18. As Fig. 14 but for (left) ^{nat}Ni$(d,x)^{56}$Co^{+} [8–10,22,23,31] including the decay of ^{56}Ni, ^{58}Ni$(d,x)^{56}$Co [28,30,32], and ^{60}Ni$(d,x)^{56}$Co reactions, and (right) ^{nat}Ni$(d,x)^{55}$Co [8–10,22–24], ^{58}Ni$(d,x)^{55}$Co [28–30,32,33], and ^{60}Ni$(d,x)^{55}$Co reactions.

Concerning the (d,α) pick-up processes, it was already obvious from the comparison of the excitation functions shown for all Ni stable isotopes in the lower part of Fig. 6 that they have the most reduced DI contributions. This feature follows the weak values for the measured α-particle angular distributions, while similar data are even missing for the ^{61,64}Ni isotopes. Moreover, these DR contribution are exceeded at incident energies higher than 40–45 MeV by the inelastic breakup contributions through (p,x) and (n,x) reactions (Figs. 14 and 15), while the statistical PE+CN α-particle emission is the dominant one for all Ni isotopes. This dominance is present also within the energy range of the (d,α) pick-up maximum, except the particular case of the ^{62}Ni$(d,x)^{60}$Co reaction (Fig. 14).

Nevertheless, the satisfactory description of all experimental ^{nat}Ni$(d,x)^{55,56,57,58,60,61}$Co excitation functions supports consistently the present analysis of the nuclear reaction mechanisms considered for description of the complex deuteron interactions.

E. The $(d,2p\alpha)$ and $(d,2\alpha x)$ reactions

The population of ^{51,52,54,56}Mn, and ^{51}Cr residual nuclei, in deuteron interaction with the ^{nat}Ni target, takes place through sizable proton and α-particle emission. The $(d,2\alpha)$ reaction leads to the first maximum of the excitation functions of the reactions ^{62}Ni$(d,x)^{56}$Mn, ^{60}Ni$(d,x)^{54}$Mn (Fig. 20), and ^{58}Ni$(d,x)^{52}$Mn (Fig. 21), while a second maximum is associated with sequential emission of nucleons and α particles at energies higher than 50 MeV. The main reaction mechanisms responsible for population of these residual nuclei are the statistical PE+CN. However, the inelastic breakup enhancement contribution remains present through the reactions $(p,p\alpha)$ (Figs. 19 and 20), and $(n,2\alpha)$ and $(p,2\alpha)$ (Fig. 22). Overall, the presently calculated excitation functions

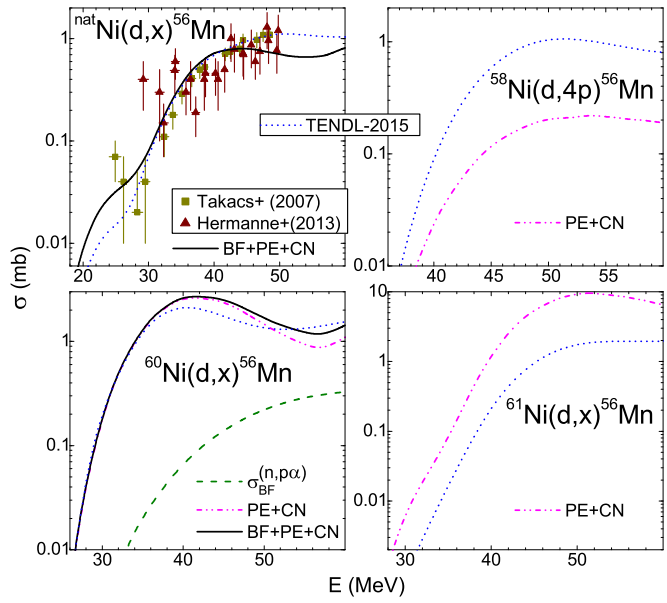

FIG. 19. As Fig. 9 but for ^{nat}Ni$(d,x)^{56}$Mn [8,10], ^{58}Ni$(d,4p)^{56}$Mn, ^{60}Ni$(d,x)^{56}$Mn, and ^{61}Ni$(d,x)^{56}$Mn reactions.

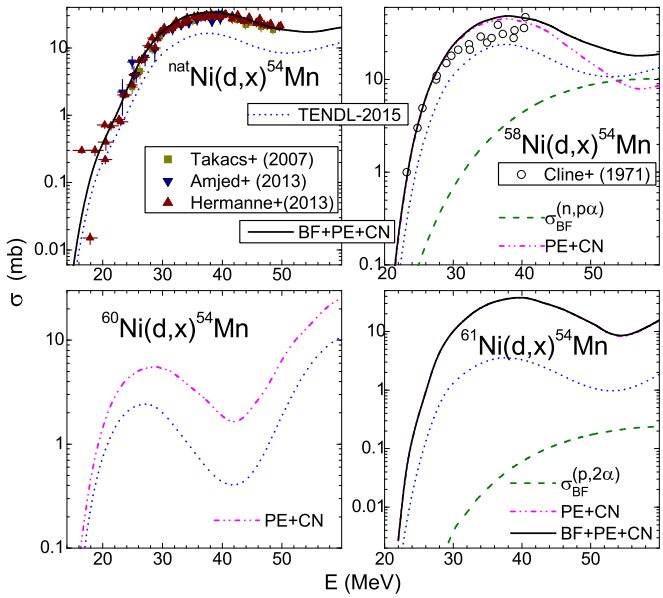

FIG. 20. As Fig. 9 but for ^{nat}Ni$(d,x)^{54}$Mn [8–10], ^{58}Ni$(d,x)^{54}$Mn [28], ^{60}Ni$(d,x)^{54}$Mn, and ^{61}Ni$(d,x)^{54}$Mn reactions.

for ^{nat}Ni$(d,x)^{52,54,56}$Mn, ^{58}Ni$(d,x)^{54}$Mn, and ^{58}Ni$(d,x)^{52}$Mn reactions show a well-improved description of the measured data [8–10,28] in comparison with the TENDL-2015 evaluation.

In a similar way to the experimental ^{nat}Ni$(d,x)^{56,57}$Co excitation functions, a cumulative process should be considered also in the case of the activation cross sections for the residual nucleus ^{51}Cr. The experimental cross sections are based on the measurements of the 320-KeV γ-ray transition of ^{51}V [80], following the decay of long-lived ^{51}Cr radionuclide ($T_{1/2} = 27.7$ days). However, because the ^{51}Cr

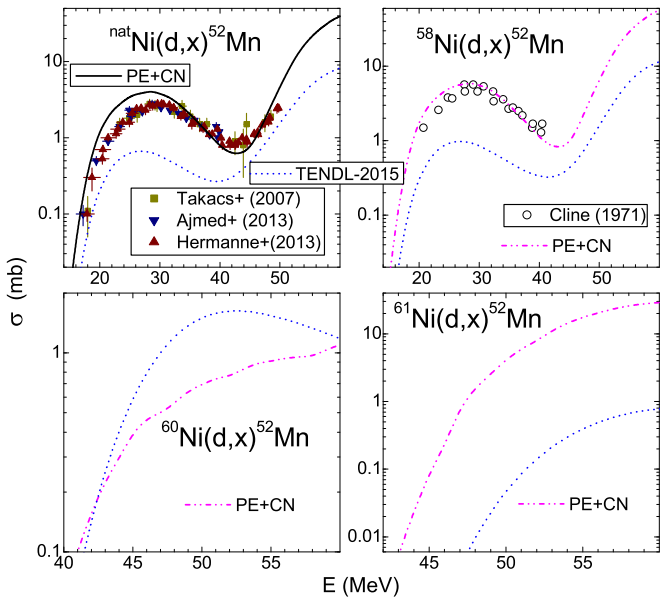

FIG. 21. As Fig. 12 but for ^{nat}Ni$(d,x)^{52}$Mn [8–10], ^{58}Ni$(d,x)^{52}$Mn [28], ^{60}Ni$(d,x)^{52}$Mn, and ^{61}Ni$(d,x)^{52}$Mn reactions.

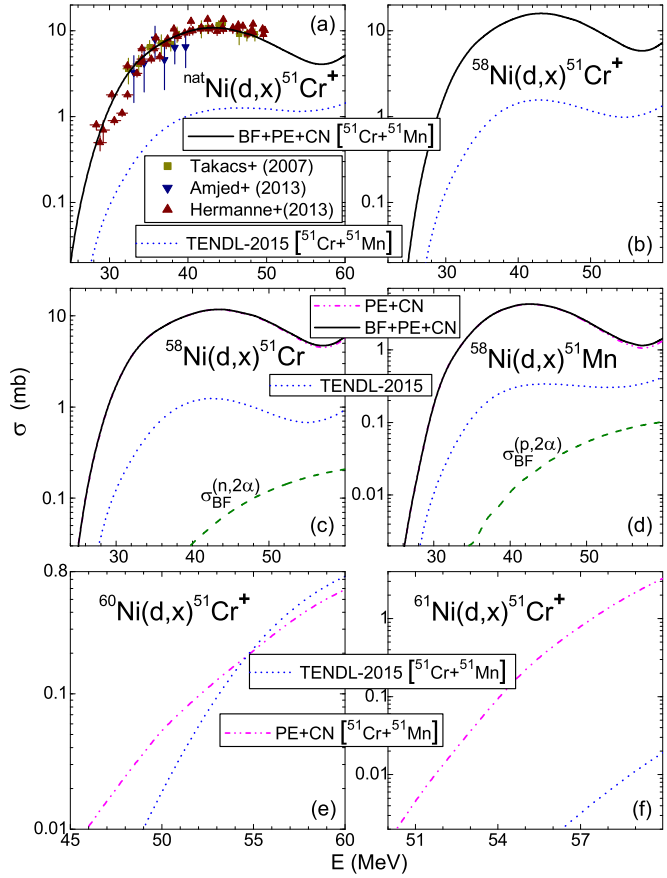

FIG. 22. As Fig. 9 but for (a) ^{nat}Ni$(d,x)^{51}$Cr, (b) ^{58}Ni$(d,x)^{51}$Cr, (e) ^{60}Ni$(d,x)^{51}$Cr, and (f) ^{61}Ni$(d,x)^{51}$Cr reactions including the decay of ^{51}Mn, as well as for (c) ^{58}Ni$(d,x)^{51}$Cr and (d) ^{58}Ni$(d,x)^{51}$Mn stand-alone reactions.

nucleus is populated also by the decay of relatively short-lived ^{51}Mn ($T_{1/2} = 46.2$ min), the measured cross sections of ^{51}Cr^{+} involve the contributions of both ^{nat}Ni$(d,x)^{51}$Cr and ^{nat}Ni$(d,x)^{51}$Mn reactions. Actually, the same situation was present for deuteron-induced reactions on Fe isotopes (see Fig. 18 of Ref. [5]). Therefore, the calculated and evaluated population of ^{51}Cr residual nucleus following the deuteron interactions with the ^{58,60,61}Ni isotopes shown in Fig. 22 include the decay of the ^{51}Mn residual nucleus. At the same time, for the target nucleus ^{58}Ni, there are shown alone the calculated and evaluated cross sections for each of the two reactions. The good agreement of the calculated and measured cross sections, versus the large underestimation of the TENDL-2015 evaluation, support once more the present analysis approach.

V. CONCLUSIONS

The activation cross sections for production of ^{55,56,57,58,58m,60}Co, ^{57,65}Ni, and ^{60,61,64}Cu radioisotopes in deuteron-induced reactions on natural Ni were measured at deuteron energies up to 20 MeV. The ^{nat}Ni$(d,x)^{65}$Ni and ^{nat}Ni$(d,x)^{58m}$Co reaction cross sections have been measured for the first time, the former being quite useful to validation

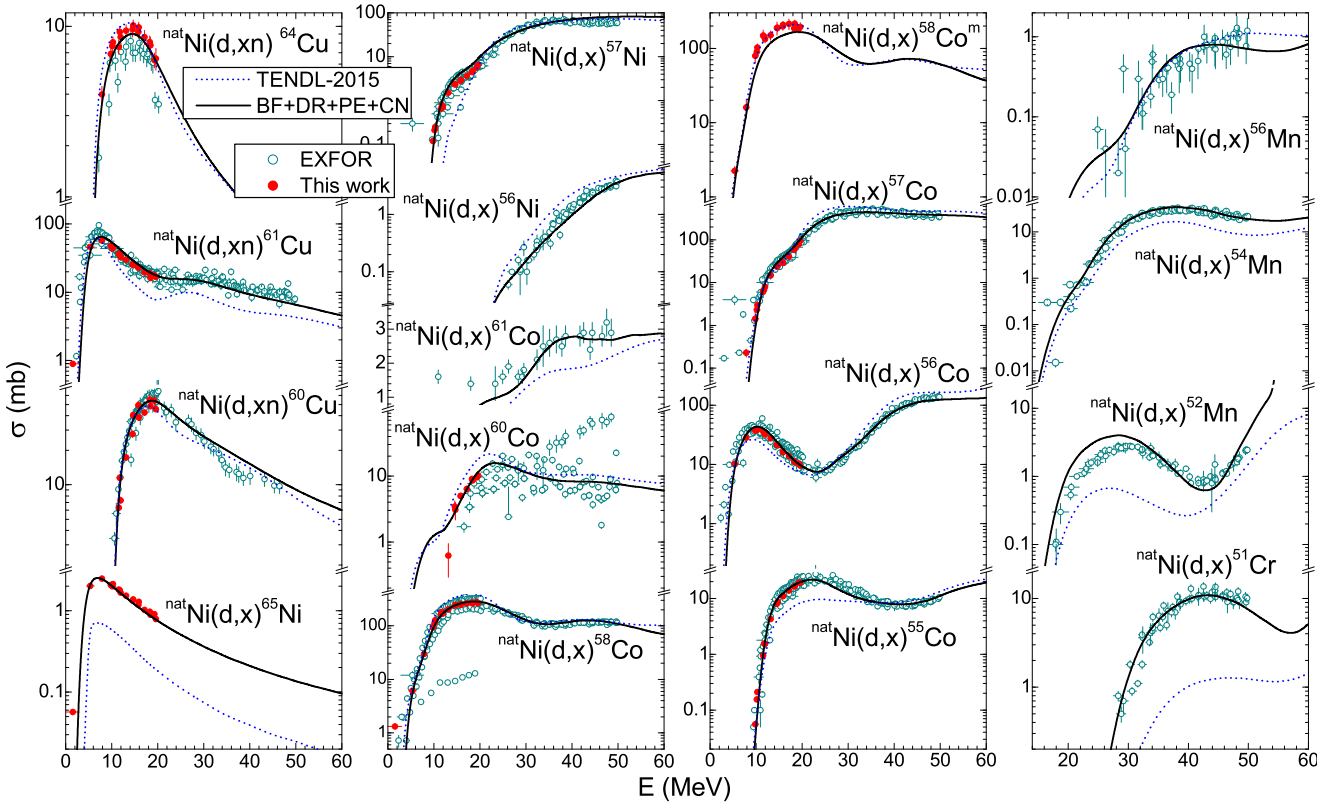

FIG. 23. Comparison of previous [8–10,22–24,31] (open circles) and present (solid circles) measurements, TENDL-2015 [17] evaluation (dotted curves), and present calculation (solid curves) of cross sections for deuteron interactions with ^{nat}Ni (see text).

of the direct reaction modeling and its role within the description of the deuteron-induced reactions. The other measurements support additionally the more recent previous data [8–10,20–24,26,28,29,31,33], enriching the experimental systematics highly requested by the large-scale research projects [11–13].

The activation data of deuteron-induced reactions on the ^{nat}Ni target, at incident energies until 60 MeV, are summarized in Fig. 23 and compared with TENDL-2015 evaluation and the model calculations carried out within the present work. All more recent data, including the present measurements, have been properly described through a unitary and consistent analysis of all reaction mechanisms, e.g., elastic scattering, breakup, stripping, pick-up, pre-equilibrium, and compound nucleus, involved in the complex deuteron interaction process. A detailed theoretical treatment of each reaction mechanism was thus proved to be necessary to obtain a reliable understanding of the interaction process as well as accurate values of calculated deuteron activation cross sections. Moreover, this detailed approach was supported by comparison of the experimental data with the present model calculations as well as the corresponding TENDL-2015 evaluation. Thus, the discrepancies between the measured and evaluated data have been explained as the result of overlooking the inelastic breakup enhancement and appropriate treatment of stripping and pick-up processes.

However, while the associated theoretical models for stripping, pick-up, PE, and CN are already settled, an increased attention should be paid to the theoretical description of the breakup mechanism, including its inelastic component. The recently increased interest on the theoretical analysis of breakup components [81–83] may lead eventually to the refinement of the deuteron breakup empirical parametrization and increased accuracy of the deuteron activation cross-section calculations. Nevertheless, the improvement of the deuteron breakup description requires, beyond the increase of its own data basis, also complementary measurements of (d,px) and (n,x), as well as (d,nx) and (p,x) reaction cross sections for the same target nucleus, within corresponding incident-energy ranges [54].

ACKNOWLEDGMENTS

This work was partly supported by Fusion for Energy (Grant No. F4E-GRT-168-02), Ministerstvo Školství, Mládeže a Tělovýchovy České Republiky (Projects No. LM2011019 and No. LM2015076), and Unitatea Executiva pentru Finantarea Invatamantului Superior, a Cercetarii, Dezvoltarii si Inovarii (Project No. PN-II-ID-PCE-2011-3-0450).

[1] M. Avrigeanu, W. von Oertzen, R. A. Forrest, A. C. Obreja, F. L. Roman, and V. Avrigeanu, Fusion Eng. Des. **84**, 418 (2009).

[2] P. Bém, E. Šimečková, M. Honusek, U. Fischer, S. P. Simakov, R. A. Forrest, M. Avrigeanu, A. C. Obreja, F. L. Roman, and V. Avrigeanu, Phys. Rev. C **79**, 044610 (2009).

[3] E. Šimečková, P. Bém, M. Honusek, M. Štefánik, U. Fischer, S. P. Simakov, R. A. Forrest, A. J. Koning, J.-C. Sublet, M. Avrigeanu, F. L. Roman, and V. Avrigeanu, Phys. Rev. C **84**, 014605 (2011).

[4] M. Avrigeanu, V. Avrigeanu, P. Bém, U. Fischer, M. Honusek, A. J. Koning, J. Mrázek, E. Šimečková, M. Štefánik, and L. Závorka, Phys. Rev. C **88**, 014612 (2013).

[5] M. Avrigeanu and V. Avrigeanu, Nucl. Data Sheets **118**, 301 (2014); M. Avrigeanu, V. Avrigeanu, P. Bém, U. Fischer, M. Honusek, K. Katovsky, C. Mănăilescu, J. Mrázek, E. Šimečková, and L. Závorka, Phys. Rev. C **89**, 044613 (2014).

[6] M. Avrigeanu and V. Avrigeanu, in *Proceedings of the 14th International Conference on Nuclear Reaction Mechanisms, 1519 June 2015, Villa Monastero, Varenna, Italy*, edited by F. Cerutti, A. Ferrari, M. Chadwick, T. Kawano, and P. Schoofs, CERN-Proceedings-2015-001 (CERN, Geneva, 2015), pp. 203–208; [http://cds.cern.ch/record/2115379].

[7] M. Avrigeanu and V. Avrigeanu, Phys. Rev. C **92**, 021601 (2015).

[8] A. Hermanne, S. Takács, R. Adam-Rebeles, F. Tárkányi, and M. P. Takács, Nucl. Instrum. Methods Phys. Res., Sect. B **299**, 8 (2013).

[9] N. Amjed, F. Tárkányi, F. Ditrói, S. Takács, and H. Yuki, Appl. Radiat. Isot. **82**, 87 (2013).

[10] S. Takács, F. Tárkányi, B. Kiraly, A. Hermanne, and M. Sonck, Nucl. Instrum. Methods Phys. Res., Sect. B **260**, 495 (2007).

[11] [http://www.iter.org/proj].

[12] [http://www.ifmif.org/b/].

[13] [http://pro.ganil-spiral2.eu/spiral2/instrumentation/nfs].

[14] Fusion Evaluated Nuclear Data Library (FENDL 3.0), [http://www-nds.iaea.org/fendl3/].

[15] I. J. Thompson, Comput. Phys. Rep. **7**, 167 (1988); computer code FRES 2.3, 2007.

[16] A. J. Koning, S. Hilaire, and S. Goriely, computer code TALYS-1.8, 2015; [http://www.talys.eu].

[17] A. J. Koning and D. Rochman, Nucl. Data Sheets **113**, 2841 (2012); A. J. Koning *et al.*, TENDL-2015: TALYS-based evaluated nuclear data library, [https://tendl.web.psi.ch/tendl_2015/tendl2015.html].

[18] J. F. Ziegler, J. P. Biersack, and M. D. Ziegler, SRIM-The Stopping and Range of Ions in Matter, computer code SRIM, [http://www.srim.org].

[19] S. Y. F. Chu, L. P. Ekström, and R. B. Firestone, The Lund/LBNL Nuclear Data, Search Version 2.0, February 1999, [http://nucleardata.nuclear.lu.se/toi/].

[20] A. Budzanowski, L. Freindl, K. Grotowski, Mrs. M. Rzeszutko, M. Slapa, J. Szmider, and P. E. Hodgson, Nucl. Phys. **49**, 144 (1963).

[21] L. Daraban, R. A. Rebeles, and A. Hermanne, Appl. Radiat. Isot. **67**, 506 (2009).

[22] J. Zweit, A. M. Smith, S. Downey, and H. L. Sharma, Int. J. of Radiation Applications and Instrumentation, Part A **42**, 193 (1991).

[23] K. Ochiai, M. Nakao, N. Kubota, S. Sato, M. Yamauchi, N. H. Ishioka, T. Nishitani, and C. Konno, in *Proceedings of the International Conference on Nuclear Data for Science and Technology, Nice, 2007*, edited by O. Bersillon, F. Gunsing, E. Bauge, R. Jacqmin, and S. Leray (EDP Sciences, Paris, 2008), p. 1011.

[24] S. Takács, M. Sonck, A. Azzam, A. Hermanne, and F. Tárkányi, Radiochim. Acta **76**, 15 (1997).

[25] M. Cogneau, L. J. Gilly, and J. Cara, Nucl. Phys. A **99**, 686 (1967).

[26] P. P. Coetzee and M. Peisach, Radiochimica Acta **17**, 1 (1972).

[27] R. Radicella, J. Rodriguez, G. B. Baro, and O. Hittmair, Z. fur Fhysik **153**, 314 (1958).

[28] C. K. Cline, Nucl. Phys. A **174**, 73 (1971).

[29] G. A. Brinkman, J. Helmer, and L. Lindner, J. Radiochemical Radioanalitical Lett. **28**, 9 (1977); EXFOR Entry No. D0162, dated 2004-07-18.

[30] Z. Fuying, T. Zhenlan, and W. Zhenxia, Chinese J. Nucl. Phys. **5**, 166 (1983); EXFOR Entry No. S0016, dated 2008-02-28.

[31] P. Jung, in *Nuclear Data for Science and Technology*, edited by S. M. Qaim (Springer-Verlag, Berlin, 1991), p. 352.

[32] M. Blann and G. Merkel, Phys. Rev. **131**, 764 (1963).

[33] N. Baron and B. L. Cohen, Phys. Rev. **129**, 2636 (1963).

[34] F. James and M. Roos, Comput. Phys. Commun. **10**, 343 (1975).

[35] W. W. Daehnick, J. D. Childs, and Z. Vrcelj, Phys. Rev. C **21**, 2253 (1980).

[36] L. L. Lee Jr., and J. P. Schiffer, Phys. Rev. **134**, B765 (1964).

[37] M. Takei, Y. Aoki, Y. Tagishi, and K. Yagi, Nucl. Phys. **472**, 41 (1987).

[38] F. Hinterberger, G. Mairle, U. Schmidt-Rohr, G. J. Wagner, and P. Turek, Nucl. Phys. **111**, 265 (1968).

[39] K. Hatanaka, K. Imai, S. Kobayashi, T. Matsusue, M. Nakamura, K. Nisimura, T. Noro, H. Sakamoto, H. Shimizu, and J. Shirai, Nucl. Phys. **340**, 93 (1980).

[40] O. Karban, A. K. Basak, F. Entezami, and S. Roman, Nucl. Phys. **366**, 68 (1981).

[41] J. K. Dickens and F. G. Perey, Phys. Rev. **138**, B1083 (1965).

[42] R. C. Brown, A. A. Debenham, J. A. R. Griffith, O. Karban, D. C. Kocher, and S. Roman, Nucl. Phys. **208**, 589 (1973).

[43] A. Auce, R. F. Carlson, A. J. Cox, A. Ingemarsson, R. Johansson, P. U. Renberg, O. Sundberg, and G. Tibell, Phys. Rev. C **53**, 2919 (1996).

[44] K. Bearpark, W. R. Graham, and G. Jones, Nucl. Phys. **73**, 206 (1965).

[45] L. V. Dubar, O. F. Nemets, L. I. Slyusarenko, and V. V. Tokarevskii, Yad. Fiz. **20**, 624 (1974); EXFOR Entry No. F0579, dated 2010-10-01.

[46] O. Bersillon, Computer code SCAT2, Note CEA-N-2227, 1992.

[47] M. Avrigeanu and A. M. Moro, Phys. Rev. C **82**, 037601 (2010).

[48] C. K. Walker, Deuteron Breakup and ^{21}Na Production, Triangle Universities Nuclear Laboratory, Durham, North Carolina, TUNL Progress Report XLII, 2002–2003, p. 82.

[49] J. Pampus, J. Bisplinghoff, J. Ernst, T. Mayer-Kuckuk, J. Rama Rao, G. Baur, F. Rosel, and D. Trautmann, Nucl. Phys. A **311**, 141 (1978).

[50] J. R. Wu, C. C. Chang, and H. D. Holmgren, Phys. Rev. C **19**, 370 (1979).

[51] J. Kleinfeller, J. Bisplinghoff, J. Ernst, T. Mayer-Kuckuk, G. Baur, B. Hoffmann, R. Shyam, F. Rosel, and D. Trautmann, Nucl. Phys. A **370**, 205 (1981).

[52] N. Matsuoka, M. Kondo, A. Shimizu, T. Saito, S. Nagamachi, H. Sakaguchi, A. Goto, and F. Ohtani, Nucl. Phys. A **345**, 1 (1980).

[53] M. G. Mustafa, T. Tamura, and T. Udagawa, Phys. Rev. C **35**, 2077 (1987).

[54] M. Avrigeanu, V. Avrigeanu, and A. J. Koning, Phys. Rev. C **85**, 034603 (2012).

[55] M. Avrigeanu and V. Avrigeanu, AIP Conf. Proc. **1645**, 139 (2015).

[56] M. Avrigeanu and V. Avrigeanu, EPJ Web of Conferences **2**, 01004 (2010); J. Phys: Conf. Ser. **205**, 012014 (2010); **533**, 012004 (2014); J. Korean Phys. Soc. **59**, 903 (2011).
[57] Experimental Nuclear Reaction Data (EXFOR), [http://www-nds.iaea.or.at/exfor].
[58] M. Kawai, M. Kamimura, and K. Takesako, Prog. Theor. Phys. Suppl. **89**, 118 (1986).
[59] P. Guazzoni, L. Zetta, A. Covello, A. Gargano, B. F. Bayman, T. Faestermann, G. Graw, R. Hertenberger, H.-F. Wirth, and M. Jaskola, Phys. Rev. C **83**, 044614 (2011).
[60] R. M. DelVecchio, Phys. Rev. C **7**, 677 (1973).
[61] Evaluated Nuclear Structure Data File (ENSDF), [http://www.nndc.bnl.gov/ensdf/].
[62] C. M. Baglin, Nucl. Data Sheets **95**, 215 (2002).
[63] K. Zuber and B. Singh, Nucl. Data Sheets **125**, 1 (2015).
[64] A. L. Nichols, B. Singh, and J. K. Tuli, Nucl. Data Sheets **113**, 973 (2012).
[65] B. Erjun and H. Junde, Nucl. Data Sheets **92**, 147 (2001).
[66] E. Browne and J. K. Tuli, Nucl. Data Sheets **111**, 2425 (2010).
[67] H. Junde, H. Su, and Y. Dong, Nucl. Data Sheets **112**, 1513 (2011).
[68] M. R. Bhat, Nucl. Data Sheets **85**, 415 (1998).
[69] C. D. Nesaraja, S. D. Geraedts, and B. Singh, Nucl. Data Sheets **111**, 897 (2010).
[70] E. Browne and J. K. Tuli, Nucl. Data Sheets **114**, 1849 (2013).
[71] M. S. Chowdhury and H. M. Sen Gupta, Nucl. Phys. A **205**, 454 (1973).
[72] J. Bommer, B. Efken, H. Fuchs, K. Grabisch, H. Kluge, W. Ribbe, G. Roschert, and F. Sichelschmidt, Nucl. Phys. A **199**, 121 (1973).
[73] H. Ohnuma, S. Takeda, N. Nakanishi, S. Yamada, M. Sekiguchi, and H. Toyama, J. Phys. Soc. Jpn. **38**, 1557 (1975).
[74] M. J. Schneider and W. W. Daehnick, Phys. Rev. C **4**, 1649 (1971).
[75] E. R. Cosman, D. N. Schramm, H. A. Enge, A. Sperduto, and C. H. Paris, Phys. Rev. **163**, 1134 (1967).
[76] T. R. Anfinsen, K. Bjorndal, A. Graue, J. R. Lien, G. E. Sandvik, L. O. Tveita, K. Ytterstad, and E. R. Cosman, Nucl. Phys. A **157**, 561 (1970).
[77] A. J. Koning and J. P. Delaroche, Nucl. Phys. A **713**, 231 (2003).
[78] F. D. Becchetti Jr., and G. W. Greenlees, *J. H. Wiliams Laboratory, University of Minnesota, Annual Report* (University of Minnesota, Minneapolis, 1969).
[79] V. Avrigeanu, M. Avrigeanu, and C. Mănăilescu, Phys. Rev. C **90**, 044612 (2014).
[80] H. Xiaolong, Nucl. Data Sheets **107**, 2131 (2006).
[81] B. V. Carlson, R. Capote, and M. Sin, arXiv:1508.01466.
[82] G. Potel, F. M. Nunes, and I. J. Thompson, Phys. Rev. C **92**, 034611 (2015).
[83] J. Lei and A. M. Moro, Phys. Rev. C **92**, 044616 (2015); **92**, 061602 (2015).